Check for updates

Application of Machine Learning and Deep EfficientNets in Distinguishing Neonatal Adrenal Hematomas From Neuroblastoma in Enhanced Computed Tomography Images

Lu Lu Xie[a, b], Ying Gong[c], Kui Ran Dong[b], Chun Shen[b, e], Bo Duan[d, e], Rui Dong[b, e]

Abstract

Background: The aim of the study was to employ a combination of radiomic indicators based on computed tomography (CT) imaging and machine learning (ML), along with deep learning (DL), to differentiate between adrenal hematoma and adrenal neuroblastoma in neonates.

Methods: A total of 76 neonates were included in this retrospective study (40 with neuroblastomas and 36 with adrenal hematomas) who underwent CT and divided into a training group (n=38) and a testing group (n=38). The regions of interest (ROIs) were segmented by two radiologists to extract radiomics features using Pyradiomics package. ML classifications were done using support vector machine (SVM), AdaBoost, Extra Trees, gradient boosting, multi-layer perceptron (MLP), and random forest (RF). EfficientNets was employed and classified, based on radiometrics. The area under curve (AUC) of the receiver operating characteristic (ROC) was calculated to assess the performance of each model.

Results: Among all features, the least absolute shrinkage and selection operator (LASSO) logistic regression selected nine features. These radiomics features were used to construct radiomics model. In the training cohort, the AUCs of SVM, MLP and Extra Trees models were 0.967, 0.969 and 1.000, respectively. The corresponding AUCs of the test cohort were 0.985, 0.971 and 0.958, respectively. In the classification task, the AUC of the DL framework was 0.987.

Conclusion: ML decision classifiers and DL framework constructed from CT-based radiomics features offered a non-invasive method to differentiate neonatal adrenal hematoma from neuroblastoma and performed better than the clinical experts.

Keywords: Neuroblastoma; Adrenal hematomas; Machine learning; Radiomics; Neonate

Introduction

Neuroblastoma is the most prevalent perinatal malignancy, with the adrenal gland being the primary site in neonates. Adrenal hematomas can manifest as cystic suprarenal masses during liquefaction, and a high incidence of cystic tumors has been previously observed among prenatally diagnosed neuroblastoma [1]. Due to the significant differences in the final treatment methods, distinguishing between the two types of lesions is crucial for subsequent diagnosis and treatment planning [2]. Furthermore, differentiating neuroblastoma complicated by hematomas from organized or calcified adrenal hematomas poses additional challenges. Generally, adrenal hematoma is a self-limiting condition that does not necessitate specific treatment [3]. However, its presence in patients can lead to potentially unnecessary surgical resection or bone marrow puncture in otherwise healthy neonates [1, 4]. Although partial or complete regression of the neuroblastoma has been observed, timely surgical removal may still be required for optimal prognosis [5]. Therefore, accurate preoperative assessment and differential diagnosis of these two types of lesions are essential for tailoring appropriate treatment decisions.

Computed tomography (CT) imaging is the most used screening method for investigating suspected adrenal occupying lesion [2]. However, due to the overlapping radiologi-

Figure 1. Workflow of this study.

cal characteristics of adrenal hematoma and neuroblastoma, imaging can sometimes lead to inconclusive results that depend primarily on physician experience [6, 7]. Radiomics is an emerging and promising field that provides comprehensive quantification of tumor types through high-throughput extraction and mining of a large number of image features [8]. With the continuous advances in computer technology and the wide range of applications of machine learning (ML) algorithms, the use of ML in medical imaging has also been increasingly valued and has been extensively applied and developed [9]. ML can extract effective features from large amounts of image data [10], build classification or regression models, identify tumor types in new samples, and assist physicians in diagnosis and prognosis evaluation [11-14].

ML algorithms have demonstrated significant utility in predicting neuroblastoma outcomes [15]. Deep learning (DL), a subset of architecture-based artificial intelligence (AI) inspired by the human brain's function and structure, encompasses convolutional neural networks (CNNs) that have been employed for fracture diagnosis [16]. In this study, we utilized radiomics to extract image features of adrenal hematomas and neuroblastomas from enhanced CT. By combining these features with clinical data, we developed appropriate feature vectors and employed ML algorithms to distinguish adrenal hematomas from neuroblastoma.

This study aimed to explore the feasibility of utilizing ML for distinguishing neonatal adrenal hematomas from neuroblastomas, providing novel ideas and methodologies to enhance the level of differential diagnosis for these two types of lesions while offering valuable references for doctors in devel-

oping more accurate treatment plans.

Materials and Methods

Description of dataset and patient population

The institutional ethics review board approved this retrospective study. This study systematically reviewed the clinical database of CT images from 40 neonates with neuroblastoma from January 2013 to January 2022 at our hospital.

Inclusion criteria were as follows: 1) patients underwent preoperative CT plain scan and two-phase enhanced scan within 3 weeks before surgery; 2) no history of radiotherapy and chemotherapy; and 3) tumors were diagnosed by postoperative pathology and had complete clinical data. The data of 36 neonates with adrenal hematomas in our hospital were included in the study. The patient inclusion criteria were as follows: 1) clinical or pathological confirmation of adrenal hematomas; and 2) imaging follow-up (complete resolution of the hematoma).

Exclusion criteria were as follows: 1) images with severe motion artifacts or evident noise; 2) maximum tumor diameter less than 1.0 cm; and 3) other tumor diseases.

We reviewed the medical records for clinical findings including age at presentation, localization of the lesion, gender, neuron-specific enolase (NSE), lactate dehydrogenase (LDH), and ferritin, and compared them between the neuroblastoma and adrenal hematomas patients. These patients were randomly separated into a training cohort and a test cohort at a 1:1 ratio.
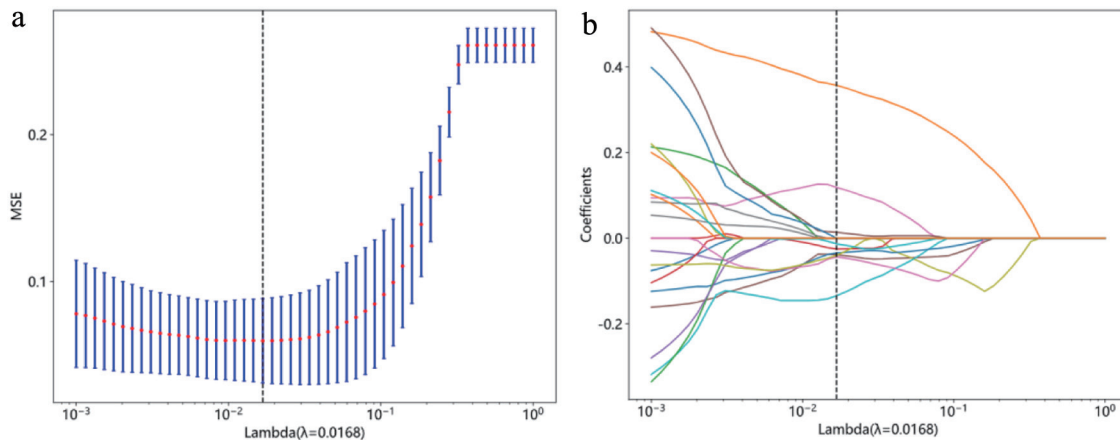
Figure 2. Radiomics feature selection with the least absolute shrinkage and selection operator (LASSO) regression model. (a) The vertical lines indicate that the optimal value of the LASSO tuning parameter λ is 0.0168. (b) LASSO coefficient profile plot with different log (λ) was shown. Nine radiomic features with non-zero coefficients were selected.

Image acquisition

All CT scans were obtained using a 64-detector row scanner (LightSpeed VCT; GE Healthcare, Chicago, IL). The scan parameters were as follows: 8,100 kV; 40 to 70 mA current; 5 mm thickness; 1.375 pitch, and field of view (FOV), 512 × 512 mm. Iodixanol was used for the enhanced CT scan (300 mg iodine/mL, dose 1.5 - 2 mL/kg, rate 1 - 3 mL/s).

Image segmentation and radiomic feature extraction

Blinded to patients' mass results, two radiologists (with 5 and 20 years of diagnostic experience) manually segmented the region of interest (ROI) respectively by using the freely available open-source software package 3D-slicer [17]. Pyradiomics library v2.2.0, as an extension of 3D-slicer, was used to extract radiomic features [18], implemented according to the consensus definition of Imaging Biomarker Standardization Initiative (IBSI), with a total of 107 quantitative features [19]. No wavelet features were incorporated. Images and data are pre-processed by resampling and standardization to ensure repeatability of results. The intra-observer and inter-observer reproducibility was evaluated by intra-class correlation coefficient (ICC). After 3 months, the radiologists performed ROI segmentation again. ICC greater than 0.9 indicated good consistency. A complete schematic is presented in Figure 1.

Classifiers and validation

Inter-group difference analysis was conducted for all features, independent sample *t*-test was used, and column standardization was carried out for features with P < 0.05 compared between groups to eliminate the impact of inter-feature scale differences. Ten-fold cross-validated least absolute shrinkage and selection operator (LASSO) regression model was used to select features with non-zero coefficients (Fig. 2). Based on

the selected features, we developed six ML models (AdaBoost, Extra Trees, gradient boosting, multi-layer perceptron (MLP), support vector machine (SVM) and random forest (RF)) to classify the patients. Compared with other CNNs, the EfficientNets has fewer parameters and is more accurate and efficient, and its baseline architecture consists of 18 convolutional layers with a resolution of 224 × 224 [20]. We applied adrenal hematoma and adrenal neuroblastoma CT images to the model for transfer learning. The network was trained for at a learning rate of 0.001 in 150 epochs.

Statistical analyses

Pearson Chi-square test or Fisher exact test was used to compare categorical variables presented as ratios between groups. The Shapiro-Wilk test was used to check if continuous variables follow a normal distribution. Comparisons of continuous variables were performed using a Student's *t*-test or Mann-Whitney U test. To evaluate the predictive performance of different models, the confusion matrix method was used to summarize the performance of ML algorithms and clinical experts during data testing, that is, to binarize all labels of the model. The diagnostic performances of these models were compared by the area under the curve (AUC) of the receiver operating characteristic curve (ROC), accuracy, sensitivity, specificity, positive prediction value (PPV), and negative prediction value (NPV). SPSS software (version 26.0, IBM) and Python software (version 3.5.6) [21] were applied for statistical analysis.

Results

Study population

A total of 76 patients were included in this study for the final analysis. Of these patients, 36 were diagnosed with adrenal hematomas either by clinical, pathological, or follow-up CT re-

Table 1. Clinical Characteristics in the Cohorts

Variable	Adrenal hematomas (N = 36)	Adrenal neuroblastoma (N = 40)	P-value
Time onset			
Prenatal	4 (11.1%)	30 (75.0%)	< 0.001*
Postnatal	32 (88.9%)	10 (25.0%)	
Sex			
Male	19 (52.8%)	25 (62.5%)	0.391
Female	17 (47.2%)	15 (37.5%)	
Localization			
Left	5 (13.9%)	15 (37.5%)	0.003*
Right	31 (86.1%)	21 (52.5%)	
Bilateral	0 (0%)	4 (10.0%)	
Weight (kg)	3.56 (3.06 - 3.98)	4.50 (3.65 - 6.50)	0.001*
NSE (ng/mL)	31.95 (22.37 - 42.17)	45.65 (26.77 - 72.30)	0.037*
Ferritin (µg/L)	573.95 (359.85 - 769.23)	318.90 (216.10 - 426.00)	< 0.001*
LDH (U/L)	667.00 (441.50 - 881.50)	299.00 (264.00 - 448.50)	< 0.001*

*$P < 0.05$. Continuous data are presented as median (interquartile range). Categorical data are presented as numbers (%). NSE: neuron-specific enolase; LDH: lactate dehydrogenase.

sults, with 40 being diagnosed with neuroblastoma. The AUC for the radiologist was calculated to be 0.831 (0.734 - 0.929) based on the report issued by the radiology department and the final clinical referral of the child. The clinical characteristics in the whole cohorts are shown in Table 1.

Radiomic signature models and performances

A total of 107 3D original radiomic features were extracted from a single ROI. These features included 18 first-order features, 14 shape features, 24 gray-level co-occurrence matrix (GLCM) features, 14 gray-level dependence matrix (GLDM) features, five neighboring gray-tone difference matrix (NGT-DM) features, 16 gray-level size zone matrix (GLSZM) features, and 16 gray-level run-length matrix (GLRLM) features.

We compared the performance of six radiomics-based ML models. Model performance results are presented in Table 2. In the test cohort, the best radiomic models were SVM, MLP, and Extra Trees, with an AUC of 0.985, 0.971 and 0.958, respectively (Table 2). The ROCs of the radiomics models in the training and test cohorts are shown in Figure 3.

Performance of DL

The mean accuracy of identifying the two kinds of adrenal lesions was 92%. The AUC for this network was 0.987. Figure 4a shows the confusion matrix of the accuracies and Figure 4b shows the AUCs. Based on the total weight parameter, a heat map was drawn according to the gradient-weighted class activation mapping (Grad-CAM) method. The heat map shows the differences related to the location of the computer-focused imaging scan (Fig. 5).

Discussion

The performance of various ML algorithms in classifying imaging data was investigated in this study. Our analysis encompassed patient data from 40 neuroblastoma and 36 adrenal hematoma cases. This represents a substantively large cohort of neonatal cases achievable at a single institution. To our knowledge, no previous study has utilized ML and DL for the differentiation of neonatal adrenal hematomas and neuroblastoma. It might offer a potentially effective non-invasive approach that is both practical and dependable for assessing adrenal tumors.

Our study demonstrates that adrenal hematomas are predominantly in the right side, while the incidence of neonatal suprarenal mass was similar between males and females, consistent with the results of Zhang et al [22]. In general, the initial suspicion of neuroblastoma occurs when a suprarenal cyst is discovered prenatally [1], and our study showed similar results. The possibility of adrenal hemorrhage cannot be excluded, even if prenatally identified adrenal cysts favor neuroblastoma. The appearance of the hematoma is very variable depending on the hemorrhagic component; therefore, they can have aspects cystic-like or solid-like [23]. Although CT can be very useful in case of adrenal hemorrhage with complex mass aspect, it is still difficult to differentiate it from neuroblastoma [24]. Currently, a consensus on imaging features to classify adrenal hematomas and neuroblastoma has not been established. Consequently, a new non-invasive method is desired to differentiate neonatal suprarenal masses.

In the field of medical imaging, radiomics is a non-invasive and powerful diagnostic method to obtain more information and uncover the genetically and pathologically heterogeneous features. Although there is currently no literature on the application of radiomics to differentiate neonatal adrenal neu-

Table 2. Diagnostic Performance of Different Models in Training and Test Cohorts

Model name	AUC (95% CI)	Accuracy	Sensitivity	Specificity	PPV	NPV
SVM						
Training	0.967 (0.900 - 1.00)	0.974	0.944	1.000	1.000	0.952
Test	0.985 (0.958 - 1.00)	0.946	1.000	0.895	0.900	1.000
RF						
Training	1.000 (1.000 - 1.000)	1.000	1.000	1.000	1.000	1.000
Test	0.937 (0.865 - 1.000)	0.892	0.778	1.000	1.000	0.826
Extra Trees						
Training	1.000 (1.000 - 1.000)	1.000	1.000	1.000	1.000	1.000
Test	0.958 (0.905 - 1.000)	0.892	0.778	1.000	1.000	0.826
Gradient boosting						
Training	1.000 (1.000 - 1.000)	1.000	1.000	1.000	1.000	1.000
Test	0.827 (0.699 - 0.956)	0.838	0.889	1.000	0.800	0.882
AdaBoost						
Training	0.967 (0.900 - 1.00)	1.000	1.000	1.000	1.000	1.000
Test	0.882 (0.771 - 0.993)	0.838	0.778	0.895	0.875	0.810
MLP						
Training	0.969 (0.921 - 1.000)	0.921	0.944	0.900	0.895	0.947
Test	0.971 (0.929 - 1.000)	0.919	0.833	1.000	1.000	0.864

CI: confidence interval; MLP: multi-layer perceptron; SVM: support vector machine; RF: random forest; AUC: area under the curve; NPV: negative prediction value; PPV: positive prediction value.

roblastoma from adrenal hematoma, it has been utilized for the prediction of response to neoadjuvant chemotherapy, genotyping, pathological classification and prognosis in neuroblastoma [15, 25-28]. In this study, the final radiomics features used to identify neuroblastoma included first-order features (2/18), shape (1/14), GLRLM (2/16), GLDM (1/14), GLCM (1/24), and NGTDM (2/5). We observed that texture features were more important than shape features, suggesting that enhanced CT image texture features were more helpful to reflect tumor heterogeneity and distinguish tumor from hematoma.
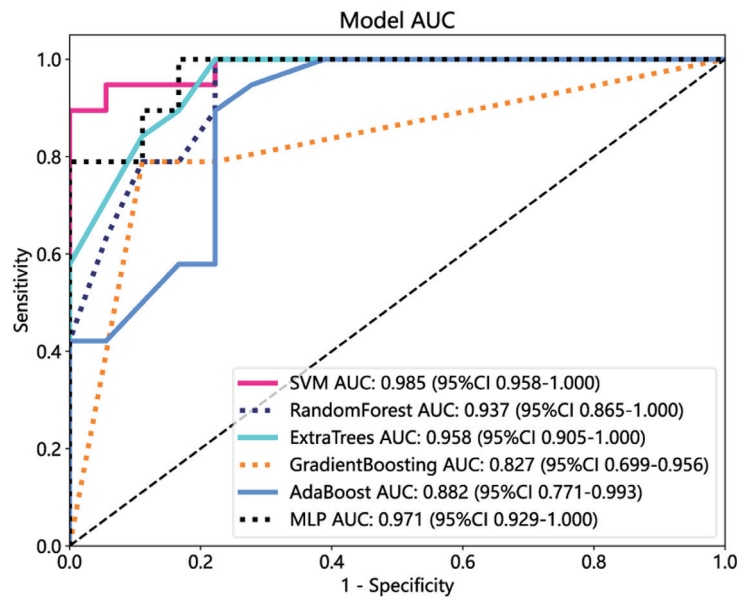
Figure 3. The receiver operating characteristic (ROC) curves of the support vector machine (SVM), random forest, Extra Trees, gradient boosting, AdaBoost, and multi-layer perceptron (MLP) in the test cohorts.
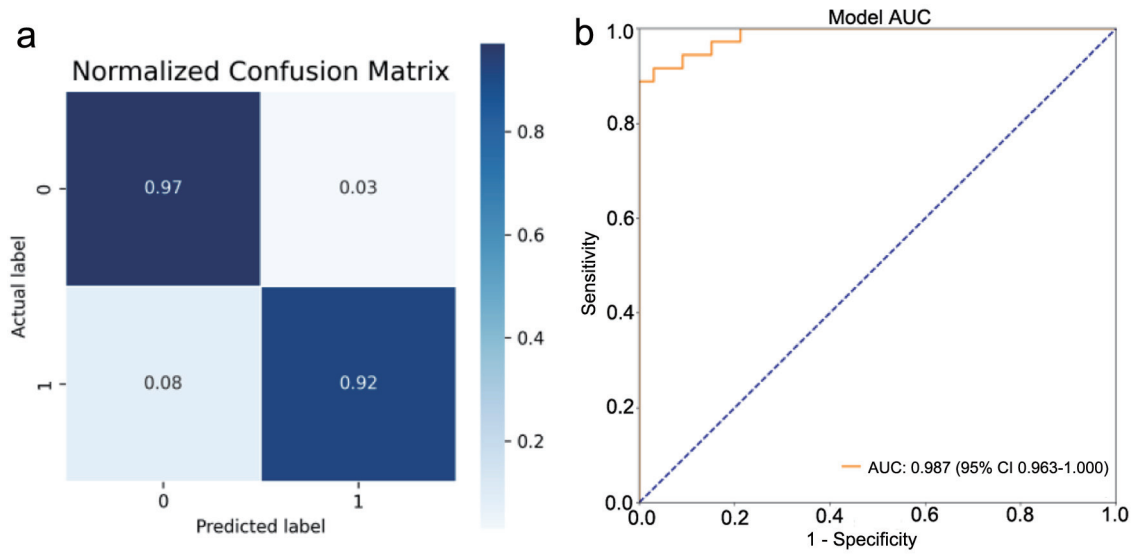
Figure 4. Performance of the lesion classification model trained with the abdominal computed tomography (CT) images. (a) Confusion matrix was drawn using the test dataset (0: neonatal adrenal hematomas; 1: neonatal adrenal neuroblastoma). (b) Image evaluation by the receiver operating characteristic (ROC) curve was drawn for neuroblastoma. Area under the curve (AUC) was calculated.
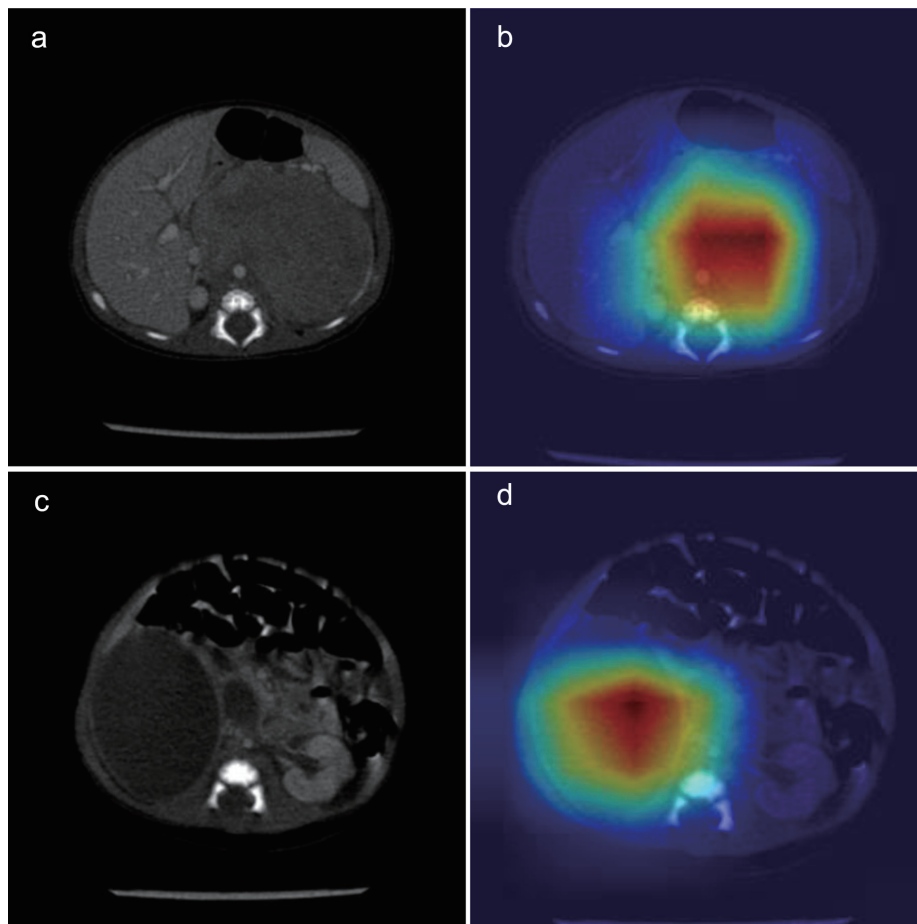
Figure 5. Computed tomography (CT) of the neonatal adrenal neuroblastoma and hematoma: original image (a, c) and heat map (b, d).

The limited number of patients in our study may have resulted in a risk of overfitting the ML-based classification model. However, previous studies have indicated that significant bias still occurs when the sample size is substantial. Therefore, we conducted data augmentation to improve class balance and prevent overfitting of the model before conducting further evaluations [29]. When the quantity of obtainable data is limited, it may require multiple attempts with different ML classifiers to identify the optimal ML approach. Compared with traditional statistical models, ML methods can automatically capture the complex relationships in the data, which is more valuable for clinical research [30], especially in building clinical prediction models [31]. Six ML-augmented approaches (AdaBoost, Extra Trees, gradient boosting, MLP, SVM, and RF) were employed. All yielded good discriminative power to correctly classify as hematomas or tumors and obtained an AUC range of 0.827 to 0.985 in the test set. This diagnostic performance surpassed the accuracy of the radiologists, who achieved an accuracy of 81.6%. SVM has satisfactory stability and efficiency, achieving almost the same performance as a large number of training samples and a few training samples [32, 33]. AdaBoost is in fact more appropriate for radiomics data because it is more robust to problems of overfitting [34] and commonly used with medical data due to its robustness with respect to noise and missing values [35].

The benefit of DL is its ability to replace manual feature acquisition with efficient algorithms for unsupervised or semi-supervised feature learning and hierarchical feature extraction. Satisfactory performances have been demonstrated in thyroid tumor classification [36], automated analysis of renal histopathology images [37], assisted reading of films for diagnosis of novel coronavirus pneumonia [38], diagnosis of fractures [16], and classification of severity of diabetic retinopathy [19]. Imaging omics analysis, as a non-invasive tool, can provide healthcare professionals with novel ideas for early diagnosis. Moreover, this technique facilitates the development of diagnostic and prognostic models for diseases, integrated with essential clinical information.

This study had several limitations. First, this study is a retrospective, single-center, and small sample size study, which uses single-machine scanning and may have potential selection bias. The relatively rarity of neonatal suprarenal mass in general makes it difficult to build a sizeable cohort without multicenter support from multiple research teams [39]. Second, the types of neuroblastomas we included were not entirely cystic. Considering the heterogeneity of the tumor and the complex situation of the hematoma [24], solid or cystic-solid masses can be used for training. In the future, more cystic adrenal lesions can be included for prospective verification. Finally, some controversy in defining the boundaries of manual segmentation relates to subjectivity [40], and 3D ROI is not clinically practical due to the long duration of segmentation. 2D ROI is easier to calculate and takes less time, but the performance of CNN on 2D neuroblastoma slices is uniformly poorer than the best performance of other ML models [15]. In the future, optimized automatic selection of image planes would help push the method toward a purely unsupervised approach, which would be ideal for clinical in-tegration [41]. This automation will enable validation of our work on large-scale datasets.

Conclusion

ML decision classifiers and DL framework constructed from CT-based radiomics features offered a non-invasive method to differentiate neonatal adrenal hematoma from neuroblastoma and performed better than the clinical experts.

Conflict of Interest

The authors have no conflict of interest to declare.

Informed Consent

The requirement of patient approval or written informed consent for reviewing medical records or images was waived.

Author Contributions

Bo Duan and Rui Dong was responsible for the conceptualization and design of this study. Bo Duan contributed to analysis and interpretation of the data. Lu Lu Xie and Ying Gong were responsible for data curation and original manuscript drafting. Kui Ran Dong and Chun Shen were responsible for the revision of the manuscript for important intellectual content. All authors read and approved the final manuscript and agreed to be accountable for the content of the work. All authors contributed to the article and approved the submitted version.

Data Availability

The datasets generated and analyzed during the current study are not publicly available due to limitations of ethical approval involving the subject data and anonymity, but are available from the corresponding author on reasonable request.

Abbreviations

AUC: area under the curve; CI: confidence interval; CNN: convolutional neural network; CT: computed tomography; Grad-CAM: gradient-weighted class activation mapping; ICC: intra-class correlation coefficient; LASSO: least absolute shrinkage and selection operator; ML: machine learning; MLP: multi-layer perceptron; ROI: region of interest; SVM: support vector machine

References

1. Eo H, Kim JH, Jang KM, Yoo SY, Lim GY, Kim MJ, Kim OH. Comparison of clinico-radiological features between congenital cystic neuroblastoma and neonatal adrenal hemorrhagic pseudocyst. Korean J Radiol. 2011;12(1):52-58. doi pubmed pmc
2. Yao W, Li K, Xiao X, Zheng S, Chen L. Neonatal suprarenal mass: differential diagnosis and treatment. J Cancer Res Clin Oncol. 2013;139(2):281-286. doi pubmed
3. Toti MS, Ghirri P, Bartoli A, Caputo C, Laudani E, Masoni F, Mele L, et al. Adrenal hemorrhage in newborn: how, when and why- from case report to literature review. Ital J Pediatr. 2019;45(1):58. doi pubmed pmc
4. Hwang SM, Yoo SY, Kim JH, Jeon TY. Congenital adrenal neuroblastoma with and without cystic change: differentiating features with an emphasis on the of value of ultrasound. AJR Am J Roentgenol. 2016;207(5):1105-1111. doi pubmed
5. Friedman DN, Goodman PJ, Leisenring WM, Diller LR, Cohn SL, Howell RM, Smith SA, et al. Long-term morbidity and mortality among survivors of neuroblastoma diagnosed during infancy: a report from the childhood cancer survivor study. J Clin Oncol. 2023;41(8):1565-1576. doi pubmed pmc
6. Badawy M, Gaballah AH, Ganeshan D, Abdelalziz A, Remer EM, Alsabbagh M, Westphalen A, et al. Adrenal hemorrhage and hemorrhagic masses; diagnostic workup and imaging findings. Br J Radiol. 2021;94(1127):20210753. doi pubmed pmc
7. Yang Shuangfeng GJLH. Imaging features of neuroblastoma in neonates. Chinese Journal of Medical Imaging. 2021. doi
8. Gillies RJ, Kinahan PE, Hricak H. Radiomics: images are more than pictures, they are data. Radiology. 2016,278(2):563-577. doi
9. Zhang B, Chang K, Ramkissoon S, Tanguturi S, Bi WL, Reardon DA, Ligon KL, et al. Multimodal MRI features predict isocitrate dehydrogenase genotype in high-grade gliomas. Neuro Oncol. 2017;19(1):109-117. doi pubmed pmc
10. Parmar C, Grossmann P, Bussink J, Lambin P, Aerts H. Machine learning methods for quantitative radiomic biomarkers. Sci Rep. 2015;5:13087. doi pubmed pmc
11. Kniep HC, Madesta F, Schneider T, Hanning U, Schonfeld MH, Schon G, Fiehler J, et al. Radiomics of brain MRI: utility in prediction of metastatic tumor type. radiology. 2019;290(2):479-487. doi pubmed
12. Temple WC, Vo KT, Matthay KK, Balliu B, Coleman C, Michlitsch J, Phelps A, et al. Association of image-defined risk factors with clinical features, histopathology, and outcomes in neuroblastoma. Cancer Med. 2021;10(7):2232-2241. doi pubmed pmc
13. Zheng YM, Li J, Liu S, Cui JF, Zhan JF, Pang J, Zhou RZ, et al. MRI-Based radiomics nomogram for differentiation of benign and malignant lesions of the parotid gland. Eur Radiol. 2021;31(6):4042-4052. doi pubmed
14. Zheng Y, Zhou D, Liu H, Wen M. CT-based radiomics analysis of different machine learning models for differentiating benign and malignant parotid tumors. Eur Radiol. 2022;32(10):6953-6964. doi pubmed
15. Liu G, Poon M, Zapala MA, Temple WC, Vo KT, Matthay KK, Mitra D, et al. Incorporating radiomics into machine learning models to predict outcomes of neuroblastoma. J Digit Imaging. 2022;35(3):605-612. doi pubmed pmc
16. Suzuki T, Maki S, Yamazaki T, Wakita H, Toguchi Y, Horii M, Yamauchi T, et al. Detecting distal radial fractures from wrist radiographs using a deep convolutional neural network with an accuracy comparable to hand orthopedic surgeons. J Digit Imaging. 2022;35(1):39-46. doi pubmed pmc
17. https://www.slicer.org.
18. van Griethuysen JJM, Fedorov A, Parmar C, Hosny A, Aucoin N, Narayan V, Beets-Tan RGH, et al. Computational radiomics system to decode the radiographic phenotype. Cancer Res. 2017;77(21):e104-e107. doi pubmed pmc
19. Zwanenburg A, Vallieres M, Abdalah MA, Aerts H, Andrearczyk V, Apte A, Ashrafinia S, et al. The image biomarker standardization initiative: standardized quantitative radiomics for high-throughput image-based phenotyping. Radiology. 2020;295(2):328-338. doi pubmed pmc
20. Sugeno A, Ishikawa Y, Ohshima T, Muramatsu R. Simple methods for the lesion detection and severity grading of diabetic retinopathy by image processing and transfer learning. Comput Biol Med. 2021;137:104795. doi pubmed
21. http://www.python.org.
22. Zhang K, Zhang Y, Zhang Y, Chao M. A retrospective analysis of the clinical characteristics of 207 hospitalized children with adrenal masses. Front Pediatr. 2023;11:1215095. doi pubmed pmc
23. Calisti A, Oriolo L, Molle P, Miele V, Spagnol L. Neonatal adrenal masses: do we have reliable criteria for differential diagnosis and expectant management? Minerva Pediatr. 2012;64(3):313-318. pubmed
24. Trinci M, Trinci CM, Galluzzo M, Rossi E, Zeccolini M, Miele V. Neonatal adrenal hemorrhage. In: Miele V, Trinci M. Imaging non-traumatic abdominal emergencies in pediatric patients. Cham: Springer International Publishing. 2016; p. 181-192.
25. Chen X, Wang H, Huang K, Liu H, Ding H, Zhang L, Zhang T, et al. CT-based radiomics signature with machine learning predicts MYCN amplification in pediatric abdominal neuroblastoma. Front Oncol. 2021;11:687884.

doi pubmed pmc

26. Wang H, Chen X, Yu W, Xie M, Zhang L, Ding H, Li T, et al. Whole-tumor radiomics analysis of T2-weighted imaging in differentiating neuroblastoma from ganglioneuroblastoma/ganglioneuroma in children: an exploratory study. Abdom Radiol (NY). 2023;48(4):1372-1382. doi pubmed

27. Wang H, Qin J, Chen X, Zhang T, Zhang L, Ding H, Pan Z, et al. Contrast-enhanced computed tomography radiomics in predicting primary site response to neoadjuvant chemotherapy in high-risk neuroblastoma. Abdom Radiol (NY). 2023;48(3):976-986. doi pubmed

28. Wang H, Xie M, Chen X, Zhu J, Zhang L, Ding H, Pan Z, et al. Radiomics analysis of contrast-enhanced computed tomography in predicting the International Neuroblastoma Pathology Classification in neuroblastoma. Insights Imaging. 2023;14(1):106. doi pubmed pmc

29. Vabalas A, Gowen E, Poliakoff E, Casson AJ. Machine learning algorithm validation with a limited sample size. PLoS One. 2019;14(11):e0224365. doi pubmed pmc

30. Karabacak M, Margetis K. Machine learning and statistics in clinical research-bridging the gap. JAMA Pediatr. 2023;177(10):1111. doi pubmed

31. Finlayson SG, Beam AL, van Smeden M. Machine learning and statistics in clinical research articles-moving past the false dichotomy. JAMA Pediatr. 2023;177(5):448-450. doi pubmed

32. Huang S, Cai N, Pacheco PP, Narrandes S, Wang Y, Xu W. Applications of support vector machine (SVM) learning in cancer genomics. Cancer Genomics Proteomics. 2018;15(1):41-51. doi pubmed pmc

33. Sanz H, Valim C, Vegas E, Oller JM, Reverter F. SVM-RFE: selection and visualization of the most relevant features through non-linear kernels. BMC Bioinformatics. 2018;19(1):432. doi pubmed pmc

34. Couronne R, Probst P, Boulesteix AL. Random forest versus logistic regression: a large-scale benchmark experiment. BMC Bioinformatics. 2018;19(1):270. doi pubmed pmc

35. Fields BKK, Demirjian NL, Hwang DH, Varghese BA, Cen SY, Lei X, Desai B, et al. Whole-tumor 3D volumetric MRI-based radiomics approach for distinguishing between benign and malignant soft tissue tumors. Eur Radiol. 2021;31(11):8522-8535. doi pubmed

36. Deng C, Li D, Feng M, Han D, Huang Q. The value of deep neural networks in the pathological classification of thyroid tumors. Diagn Pathol. 2023;18(1):95. doi pubmed pmc

37. Koo JC, Ke Q, Hum YC, Goh CH, Lai KW, Yap WS, Tee YK. Non-annotated renal histopathological image analysis with deep ensemble learning. Quant Imaging Med Surg. 2023;13(9):5902-5920. doi pubmed pmc

38. Mzoughi H, Njeh I, Slima MB, BenHamida A. Deep efficient-nets with transfer learning assisted detection of COVID-19 using chest X-ray radiology imaging. Multimed Tools Appl. 2023;82:39303-39325. doi pubmed pmc

39. Bluemke DA, Moy L, Bredella MA, Ertl-Wagner BB, Fowler KJ, Goh VJ, Halpern EF, et al. Assessing radiology research on artificial intelligence: a brief guide for authors, reviewers, and readers-from the radiology editorial board. Radiology. 2020;294(3):487-489. doi pubmed

40. Lohmann P, Bousabarah K, Hoevels M, Treuer H. Radiomics in radiation oncology-basics, methods, and limitations. Strahlenther Onkol. 2020;196(10):848-855. doi pubmed pmc

41. Zhang J, Zhan C, Zhang C, Song Y, Yan X, Guo Y, Ai T, et al. Fully automatic classification of breast lesions on multi-parameter MRI using a radiomics model with minimal number of stable, interpretable features. Radiol Med. 2023;128(2):160-170. doi pubmed